Anisotropy effects in superconducting niobium

H.W. Weber, E. Seidl, and C. Laa
Atominstitut der Österreichischen Universitäten, A-1020 Wien, Austria

E. Schachinger and M. Prohammer
Institut für Theoretische Physik, Technische Universität Graz, A-8010 Graz, Austria

A. Junod and D. Eckert
Département de Physique de la Matière Condensée, Université de Genève, CH-1211 Genève 4, Switzerland
(Received 17 December 1990)

This paper presents an extensive experimental and theoretical analysis of anisotropy effects in superconducting niobium. It is concluded that anisotropy effects, especially in the magnetic properties, are clearly discernible and that the theoretical analysis results in a mean-square anisotropy of the electron–phonon interaction of 0.0335 ± 0.0035 and of the Fermi velocity of 0.118 ± 0.007. These anisotropy parameters are in excellent agreement with previous de Haas – van Alphen experiments.

I. INTRODUCTION

Anisotropy effects in superconducting niobium have been well known for many years and are probably most apparent in the angular dependence of the upper critical magnetic field, H_{c2}, in high purity single crystals as a function of the orientation of the applied magnetic field with respect to the crystal axis. However, they become also apparent in the temperature dependence of the thermodynamic critical field H_c ("deviation function"), the temperature dependence of the specific heat, the functional dependence of upper critical fields, H_{c2}, near T_c, and the magnitude of the Ginzburg-Landau parameters, especially at low temperatures. All of these features were found to depend distinctly on the amount of impurity scattering prevailing in a particular superconductor and to approach the expected isotropic behavior at a certain (low) impurity level. It is well understood that this anisotropy is related to the anisotropy of the Fermi surface of the real metal, which manifests itself in an anisotropic Fermi velocity and in an anisotropic electron-phonon interaction. Quite some effort was dedicated to an unambiguous assessment of the existence and magnitude of the anisotropy in the pairing interaction, a task which depends heavily on the theoretical interpretation of experimental data.

The first important step in that direction was made by Peter *et al.*,[1] who calculated the critical temperature of niobium using band-structure results and an experimental phonon spectrum. In this study, the anisotropy in the electron-phonon interaction turned out to be crucial for the quality of the theoretical result.

Butler,[2] on the other hand, concentrated on the upper critical magnetic field of niobium single crystals using strong coupling equations by Eilenberger and Ambegaokar[3] and extensive band-structure calculations. His key assumption was that the anisotropy of the Fermi velocity was the dominant feature and that the anisotropy of the upper critical field directly reflected the anisotropy of the Fermi surface. His results agreed very well with experimental data reported by Kerchner *et al.*[4]

A different approach was presented by Teichler[5] who developed a theory of the upper critical field which is applicable to all cubic type-II superconductors. In this description the angular dependence of H_{c2} is expressed in terms of normalized cubic harmonics which makes an interpretation of the results rather tedious. After an initial quite reasonable agreement with experiment,[6] improved experimental techniques[7] revealed that the agreement was less satisfying, and in some cases the experimental trends were inconsistent with theoretical predictions.

This paper presents extensive investigations of anisotropy effects in the superconducting properties of a very pure niobium single crystal and of niobium polycrystals of various nitrogen content. The critical temperature and its impurity dependence, the specific heat and the temperature dependence of the upper critical magnetic field were measured for all samples and the results were analyzed later on using anisotropic Eliashberg theory in an attempt to establish the mean-square anisotropies of the electron-phonon interaction and of the Fermi velocity. Thus, Sec. II presents details of sample preparation and of the measuring techniques, Sec. III discusses the basic superconducting and normal-state properties. In Sec. IV, an analysis of the experimental data in terms of anisotropic Eliashberg theory is discussed in great detail and the consistency of the derived anisotropy parameters is checked against other experiments. In Sec. V conclusions are drawn.

II. EXPERIMENTAL

A. Sample preparation

Several polycrystalline rods and a single crystal, all of nominally very high purity niobium (Materials Re-

search Corp., New York), were cut into cylindrical form (3-mm diameter, 40-mm length) using a spark cutter and subjected to an initial heat treatment in an UHV system, in order to remove residual gaseous impurities ($T = 2100\,°C$, base pressure of the system: 10^{-11} mbar). Special care was taken to remove carbon from the samples. This was achieved by exposing them to an oxygen atmosphere ($p_{O_2} = 10^{-8}$ mbar) at a temperature of 1690 °C. After these preparatory steps, the polycrystals were loaded with varying amounts of nitrogen in order to achieve the desired impurity variation within this system. The dissolution of nitrogen in niobium was achieved at a fixed temperature (2100 °C) and for a fixed period of time (4 h) under varying nitrogen partial pressures (6×10^{-7} to 1×10^{-4} mbar), which led to impurity concentrations between 0.01 and 0.5 at. % N_2. Special care was taken to cool the samples to room temperature rather quickly in order to avoid precipitate formation. The nitrogen content of the samples was determined from their weight increase under due consideration of niobium evaporation losses. Next, the samples were etched briefly in a 1:1:1 solution of HNO_3, HF, and H_2O in order to remove impurities from the surface. Finally, all samples were subjected to a short heat treatment in air (400 ° C, 10 min), a procedure[8] which has been found to considerably reduce irreversibilities in the magnetization.

B. Measuring techniques

In order to characterize the materials and to determine the relevant superconductive parameters, several techniques have been employed. Firstly, conventional four-point dc measurements were made at room temperature and at 4.2 K ($H > H_{c2}$), in order to determine the resistivities (ρ_n) and the residual resistivity ratios (RRR) of the samples. Whereas the RRR values, which have been corrected for magnetoresistivity in the clean samples, are considered accurate, the accuracy of the normal state resistivities is determined mainly by the extent to which the actual geometry of the samples can be assessed. The corresponding error margin is estimated to be ±2%.

Secondly, ac susceptibility measurements were made on some samples in order to determine the superconducting transition temperature T_c and/or the upper critical field H_{c2}. However, because the results obtained from this technique were found to be in excellent agreement with those derived from magnetization measurements,[9] the ac susceptibility data were used only as confirmatory evidence for the procedures employed to evaluate the magnetization data.

Thirdly, the dc magnetization was measured on all samples in the temperature range from 1.5 K to T_c. To do this, a differential technique employing a low-temperature voltage chopper in connection with a two-channel lock-in amplifier[10] was used. The advantages of this system with regard to the evaluation of various mixed state properties of superconductors has been discussed in much detail recently;[11–13] they are mainly based on the excellent long-term stability and the low drift of the entire system, which allows very low field-sweeping rates (10–100 $\mu T s^{-1}$) to be employed and, hence, to minimize eddy current contributions and to achieve equilibrium conditions in the entire magnetization cycle. All the data were stored on a computer and were available for numerical analysis. Two examples of integrated magnetization curves are shown in Fig. 1. They demonstrate in fact that the magnetization curves are sufficiently reversible for a reliable evaluation of the mixed-state properties, except for some irreversibilities occurring invariably near H_{c1} and, for the less pure samples, in the form of small peak effects near H_{c2}. The resolution for determining H_{c2} from the differential curve is in general better than ± 0.5 mT.

Finally, measurements of the specific heat have been taken on five samples representing the entire range of impurity parameters covered in this study. The calorimeter arrangement used for these measurements is of the "tray" type, i.e., the sample is placed onto a thick sapphire platform which carries the thermometer and the heater on its back. Thermal contact to the cylindrical samples has been made by a small amount (mg) of silicone grease and thin copper wires. The heat capacity of the entire sample holder excluding the sample was measured separately and subtracted later on. Its contribution amounts

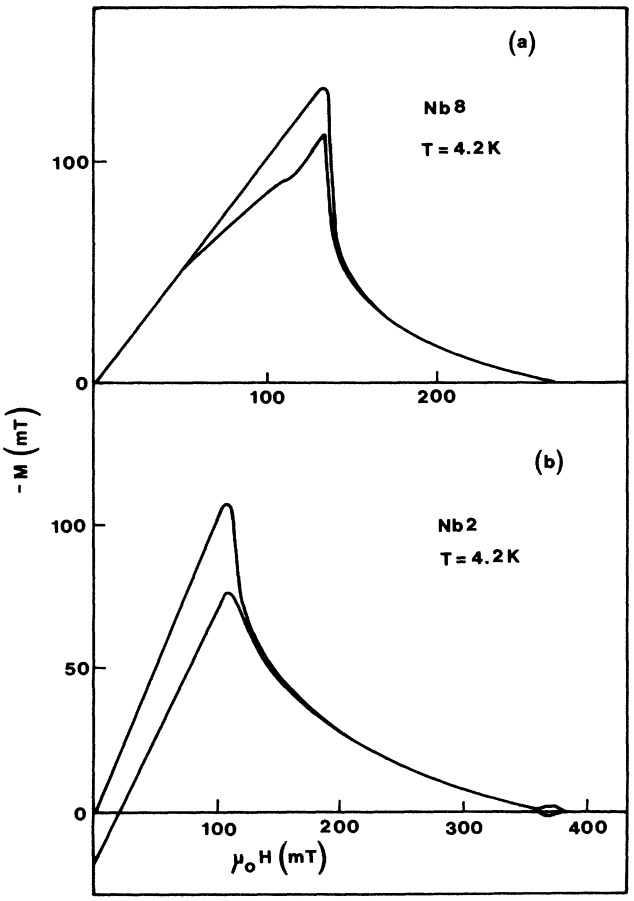

FIG. 1. Integrated (differential) magnetization curves of samples Nb_8 and Nb_2 for the initial magnetization and for decreasing fields.

to less than 3% at 8 K for Nb samples weighing 1.6 – 2.3 g. The carbon thermometer was calibrated *in situ* immediately before each measurement at 45 – 60 equally spaced temperatures (on a logarithmic scale) using both vapor pressure (T_{58}) and gas thermometer scales. A mechanical heat switch was used during this phase of the experiment rather than exchange gas in order to avoid later heat leaks due to desorption. The measurements are based on a semiadiabatic heat pulse technique which yields an accuracy of the order of 1%. All the experiments were performed in zero magnetic field.

III. BASIC SUPERCONDUCTIVE AND NORMAL STATE PROPERTIES

A. Impurity concentration and residual resistivity

The first set of data to be presented in this section pertains to the impurity dependence of the normal state resistivity at 4.2 K, which is considered to be a rather sensitive test of sample preparation with regard to an interstitial dissolution of the nitrogen impurities. The results shown in Fig. 2 confirm that ρ_n increases linearly with impurity concentration, at least within experimental accuracy (the error bars associated with ρ_n are smaller than the symbols and the errors in the impurity concentration, c_i, are not known).

If there is only s-wave scattering by nonmagnetic impurities, it is possible to employ a "dressed" Drude theory and thereby relate the normal state resistivity to the transport relaxation time, τ_{tr}, via the plasma frequency Ω_p:

$$\rho_n = \frac{4\pi}{\tau_{tr}\Omega_p^2}\,, \tag{1}$$

$$\Omega_p^2 = 4\pi \langle v_F \rangle^2 N(0)\, e^2/3, \tag{2}$$

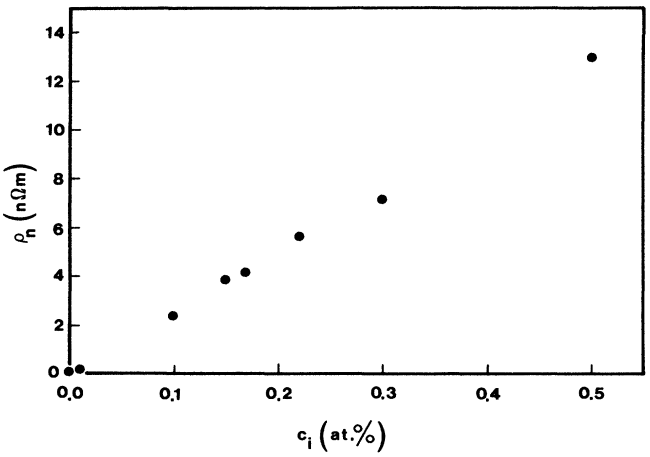

FIG. 2. Residual resistivity ρ_n as a function of nitrogen content c_i.

where $N(0)$ denotes the experimental density of states at the Fermi surface and $\langle v_F \rangle$ is the Fermi surface average of the Fermi velocity. The results of these calculations (for a more detailed description we refer to Sec. IV) are in very close agreement with the actual experimental data, as can be seen in Table I, thus indicating that s-wave scattering is indeed prevailing. The same conclusion has been drawn recently from an analysis of phase boundaries in superconducting tantalum.[11,14] (Table I also defines unique sample numbers which identify the samples with their nitrogen content.)

Finally, based on these considerations, the electron mean-free path ℓ can be calculated by assuming that the product $\langle \rho_n \ell \rangle$ will remain unchanged upon adding the impurities[15] ($\langle \rho_n \ell \rangle = 3.75 \times 10^{-16}\ \Omega\mathrm{m}^2$ for niobium). The corresponding results for ℓ are also included in Table I.

TABLE I. Characteristic data of the various samples. c_i is the nitrogen content in at. %, RRR is the residual resistivity ratio, ρ_n the experimental value of the residual resistivity at $T = 4.2$ K in nΩm, ρ_{theor} the theoretical value of the residual resistivity, calculated from Eq. (32), T_c the bulk critical temperature in K, $\kappa(T_c)$ the Ginzburg-Landau parameter, α the impurity parameter, ℓ the mean-free path in nm, $\langle a^2 \rangle$ and $\langle b^2 \rangle$ are dimensionless, and $\langle v_F \rangle$ the Fermi surface average of the Fermi velocity in 10^6 m/s.

Sample	Nb_8	Nb_7	Nb_4	Nb_3	Nb_5	Nb_2	Nb_6
Crystal	Single	Poly	Poly	Poly	Poly	Poly	Poly
c_i		0.01	0.10	0.15	0.22	0.30	0.50
RRR	2080	385	57	38	26	20	11
ρ_n	0.069	0.257	2.433	3.815	5.637	7.076	12.972
ρ_{theor}	0.093	0.381	2.44	3.587	5.429	7.325	
T_c	9.301	9.289	9.218	9.187	9.146	9.112	8.989
κ	0.720	0.725	0.883	0.917	1.090	1.153	1.453
	±0.007	±0.01	±0.049	±0.015	±0.015	±0.045	±0.027
α	0.011	0.02	0.278	0.421	0.616	0.719	1.208
ℓ	5149	1459	154	98	67	53	29
$\langle a^2 \rangle$		0.037	0.037	0.037	0.034	0.036	
$\langle b^2 \rangle$		0.112	0.118	0.125	0.125	0.125	
$\langle v_F \rangle$		0.585	0.573	0.560	0.558	0.560	

B. Transition temperatures and Ginzburg-Landau parameters

The superconducting transition temperatures of all the samples were determined by extrapolating the upper critical fields H_{c2} obtained from the dc magnetization to zero. To do this, several measurements (usually about 10) were made very close to T_c ($0.97T_c \leq T < T_c$) and the corresponding results extrapolated by fitting them to a $H_{c2}(T)$ versus T^2 temperature dependence. The agreement with ac susceptibility measurements was very good. The error in T_c is basically determined by the calibration error of the Ge thermometer and is estimated to be ± 4 mK. The results are shown in Fig. 3. The smooth dependence of T_c on impurity content again seems to confirm that the impurities have been dissolved interstitially, with the exception of the sample with the highest impurity content (Nb_6) whose T_c falls considerably below the expected value. The reasons for this deviation are unclear, especially in view of the fact that weighing uncertainties become rather small at higher nitrogen concentrations. In addition, if precipitate formation, which becomes more likely at higher impurity levels, is assumed to be responsible, the opposite trend, i.e., a higher T_c, would be expected. A detailed discussion of the results in terms of anisotropy removal by impurity scattering will be presented in Sec. IV.

With regard to an experimental assessment of the Ginzburg-Landau parameters $\kappa_1(T)$, $\kappa_2(T)$, and κ,

$$\kappa_1(T) = \frac{H_{c2}(T)}{\sqrt{2}H_c(T)} , \tag{3}$$

$$\kappa_2(T) = \frac{1}{\sqrt{2}}\left(1 + \frac{1}{1.16(\mathrm{d}M/\mathrm{d}\mu_0 H)|_{H_{c2}}} - \frac{D}{1.16}\right)^{1/2} , \tag{4}$$

$$\kappa = \kappa_1(T_c) = \kappa_2(T_c), \tag{5}$$

the following procedures were adopted.[16] In a differential magnetization measurement, both $H_{c2}(T)$ and the slope of the magnetization at H_{c2} are directly accessible to experiment and can, therefore, be determined with high accuracy. On the contrary, the thermodynamic critical field H_c must be determined by a twofold integration of the experimental data, which can result in substantial error margins. In addition, H_c (i.e., the area under the integrated differential magnetization curve) is most sensitive to residual hysteresis effects. Hence, once the demagnetization factor D has been established in a satisfactory way,[11] $\kappa_2(T)$ is certainly the quantity which can be assessed from experiment with the highest accuracy. It turned out [Fig. (4b)], that κ_2 varied linearly with

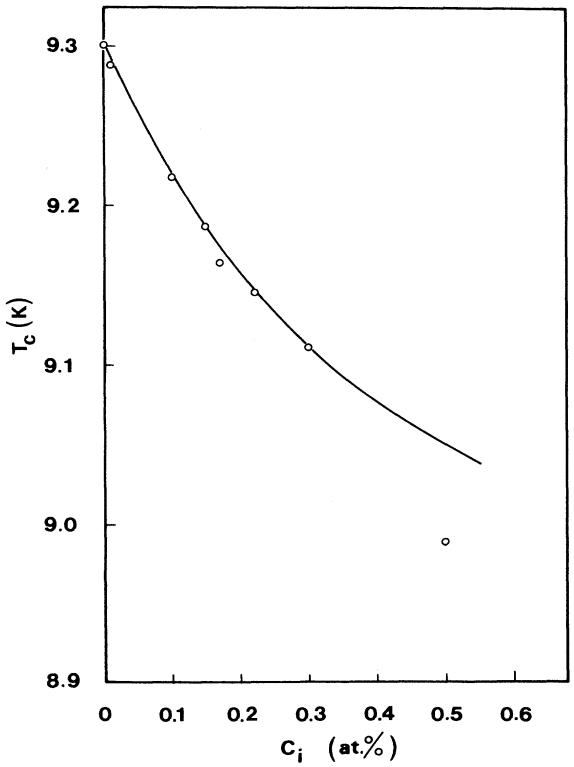

FIG. 3. Critical temperatures of niobium samples as a function of nitrogen content c_i.

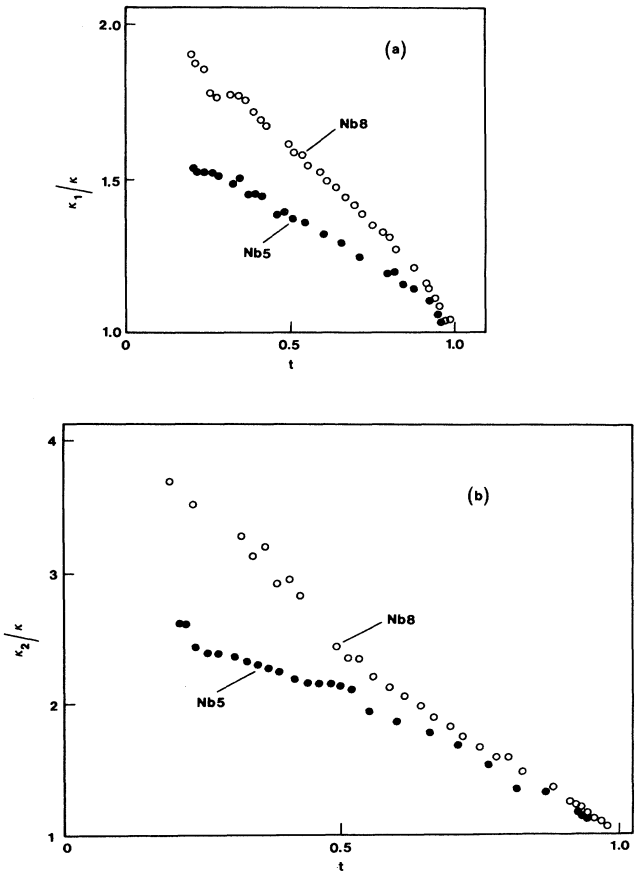

FIG. 4. (a) κ_1 as a function of the reduced temperature $t = T/T_c$ for various samples. (b) The same for κ_2.

temperature close to T_c in all the samples investigated. Hence, to determine the Ginzburg-Landau parameter κ for each sample, a similar procedure to that described above for the evaluation of T_c was employed. The corresponding results are listed in Table I.

The temperature and impurity dependence of the Ginzburg-Landau parameters (Fig. 4) has been discussed in much detail recently,[11] brief reference to a comparison of the experimental κ_1 data with anisotropic Eliashberg theory will be made in Sec. IV. In the following we will

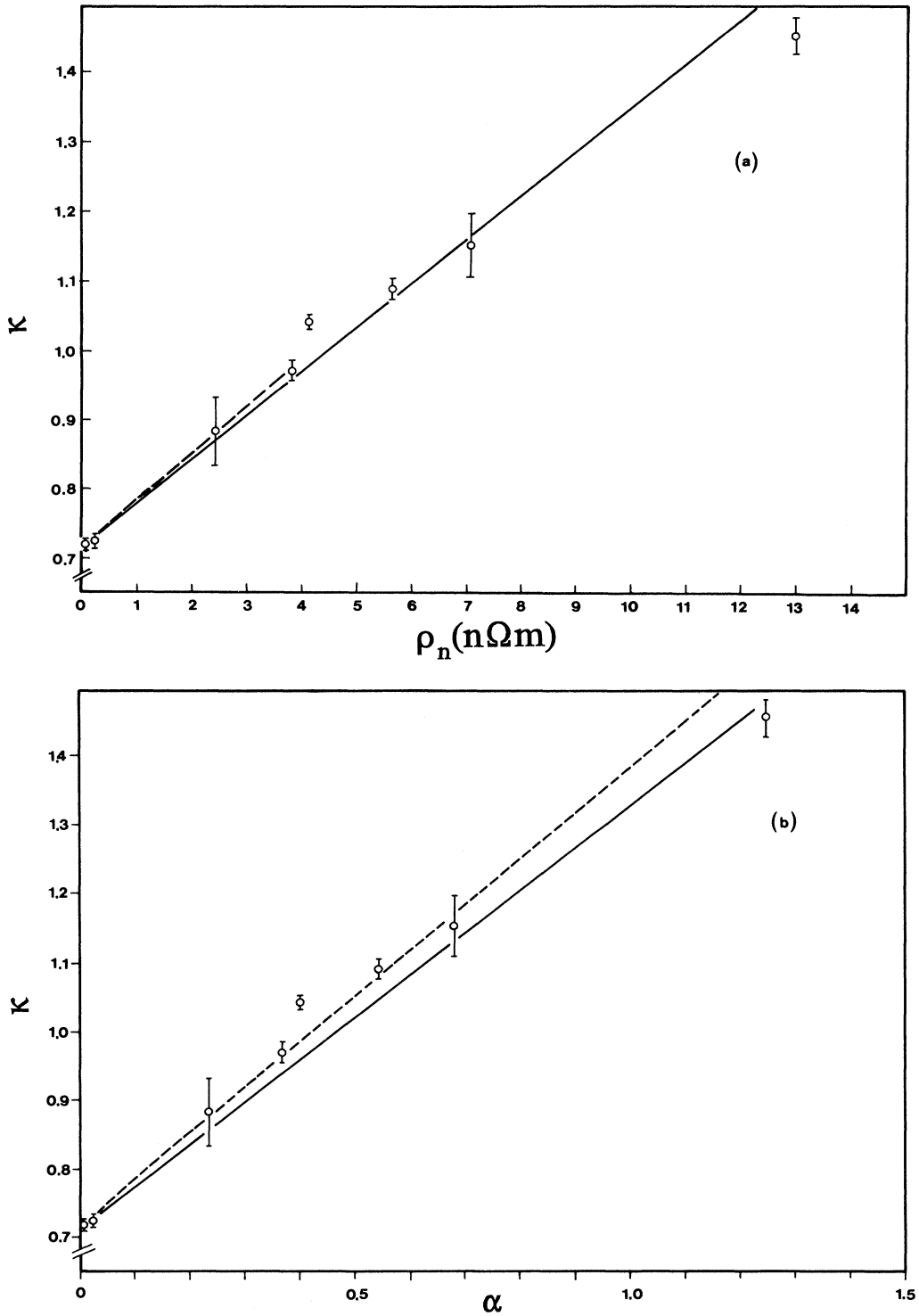

FIG. 5. Ginzburg-Landau parameters κ as a function of the residual resistivity ρ_n (a), and impurity parameter α (b). (a) Dashed line: linear regression through the experimental data to determine κ_0, solid line: Gor'kov-Goodman relation. (b) Dashed line: Gor'kov function, solid line: Gor'kov-Goodman relation.

restrict ourselves to a discussion of the impurity dependence of κ in terms of the Gor'kov-Goodman relation[17] and the Gor'kov function $\chi(\alpha)$.[18] The experimental results correlating the Ginzburg-Landau parameters with measured normal state resistivities are shown in Fig. 5(a). In order to determine the clean-limit ($\rho_n = 0$) value of κ, a linear regression was fitted through the four data points pertaining to the samples with the lowest resistivities. This results in a clean-limit value of $\kappa_0 = 0.713$, which is just barely above the limiting value (0.707) for type-II superconductivity. It should be noted that the determination of κ_0 as decribed above is a purely experimental procedure and based on the availability of a series of samples with varying impurity content at very low impurity concentrations. This result for κ_0 together with the experimental value for the Sommerfeld constant ($\gamma = 720\ \mathrm{J\,K^{-2}\,m^{-3}}$, cf. below) can be used to evaluate the Gor'kov-Goodman relation

$$\kappa = \kappa_0 + 2.37 \times 10^6 \gamma^{1/2} \rho_n \tag{6}$$

(γ in $\mathrm{J\,K^{-2}\,m^{-3}}$, ρ_n in Ωm), which is shown by the solid line in Fig. 5(a). Clearly, the overall agreement between experiment and Eq. (6) is very good (maximum deviation: 3%), and even better than the theoretically estimated accuracy (6%) of Eq. (6).

As the next step, the impurity parameter $\alpha = 0.882\xi_0/\ell$ (ξ_0 is the clean-limit coherence length and ℓ the electron mean-free path) can be calculated, which may be done in three ways. Firstly, the ℓ values obtained from the resistivity (cf. Sec. III A) and ξ_0 (= 38.9 nm, cf. below) can be used directly to calculate α. This is shown by the symbols in Fig. 5(b). Secondly, α can be evaluated numerically from the Gor'kov function

$$\kappa = \kappa_0/\chi(\alpha)\ , \tag{7}$$

$$\chi(\alpha) = \frac{8}{7\zeta(3)} \sum_{n=0}^{\infty} \frac{1}{(2n+1)^2(2n+1+\alpha)}, \tag{8}$$

using the clean-limit result for κ_0 (=0.713). This data is shown by the dashed line in Fig. 5(b) and listed in Table I. Thirdly, the mean-free path ℓ can be calculated from Eq. (6) in a slightly modified form[17] and used again in conjunction with ξ_0 to evaluate α:

$$\kappa = 0.96\lambda_L(0)\left(\frac{1}{\xi_0} + \frac{1}{1.327\ell}\right) = \kappa_0 + \frac{\kappa_0\xi_0}{1.327\ell} \tag{9}$$

with

$$\ell = \frac{\xi_0\kappa_0}{1.327(\kappa - \kappa_0)}\ . \tag{10}$$

This data is shown as the solid line in Fig. 5(b). Clearly, all of these procedures yield results which are very close together and, thus, basically confirm the validity of the approaches outlined above. Note, however, that slightly different slopes of the κ-α dependence are obtained. Hence, if only one sample is available for the analysis and if the Gor'kov-Goodmann relation is employed to extrapolate the Ginzburg-Landau parameter to $\alpha = 0$, then the flatter slope of this approximation will invariably lead to an overestimation of κ_0. Therefore, the results presented in Fig. 5(b) explain the consistently higher values of κ_0 for niobium published so far.[4,19,20]

Finally, we wish to summarize briefly the data on clean-limit parameters for niobium, which were obtained by employing standard BCS relations. From the measured slopes of the critical fields H_{c2} and H_c at T_c,

$$-\left.\frac{\mathrm{d}\mu_0 H_{c2}}{\mathrm{d}t}\right|_{t=1} = 400 \pm 2\ \ \mathrm{mT}\ , \tag{11}$$

$$-\left.\frac{\mathrm{d}\mu_0 H_c}{\mathrm{d}t}\right|_{t=1} = 395 \pm 2\ \ \mathrm{mT}, \tag{12}$$

where t is the reduced temperature, $t = T/T_c$, we obtain the Fermi velocity

$$\left(\frac{\langle (v_F^*)^2\rangle}{(1+\lambda)^2}\right)^{1/2} = (2.768 \pm 0.008) \times 10^5\ \mathrm{m/s} \tag{13}$$

and the clean–limit coherence length ξ_0^*

$$\xi_0^* = 0.18\frac{\hbar}{k_B T_c}\left(\frac{\langle (v_F^*)^2\rangle}{(1+\lambda)^2}\right)^{1/2} = 40.9 \pm 0.1\ \ \mathrm{nm}, \tag{14}$$

where the $*$'s indicate that the energy dependence of the gap function according to Butler,[2] leading to an enhancement factor $e_{SC} = 1.104$ in the slope of H_{c2}, has been included in the evaluation. The corresponding values without this correction are $\sqrt{\langle v_F^2\rangle/(1+\lambda)^2} = 2.634\times10^5$ m/s and $\xi_0 = 38.9$ nm, respectively. Furthermore, the zero-temperature penetration depth $\lambda_L(0)$ is obtained from the slope of H_c, $\lambda_L(0) = 29.0 \pm 0.2$ nm, in excellent agreement with the clean limit result for κ_0,

$$\lambda_L(0) = \frac{\xi_0\kappa_0}{0.96} = 28.9 \pm 0.1\ \ \mathrm{nm}. \tag{15}$$

C. Specific heat

The single crystal (Nb_8) was measured in the temperature range from 1.3 to 50 K and four polycrystalline samples (Nb_7, Nb_4, Nb_5, and Nb_6) were measured from 1.2 to 20 K. The results are shown in Fig. 6. They demonstrate that the nitrogen doping results in a *bulk* depression of the critical temperature T_c and in limited smearing of the transition width.

Quantities given by the theoretical anlaysis (e.g., condensation energy) are related to differences between the normal state and superconducting state data. Since only zero-field measurements were performed, a detailed description of the procedures employed to obtain the normal-state data is in order. A straight extrapolation of C/T versus T^2 from above T_c would lead to erroneous results, since an anomaly is known to occur near 3 K in the slope of the lattice specific heat.[21] Therefore, we have to allow for some curvature and fit a more general curve, using numerous constraints to secure extrapola-

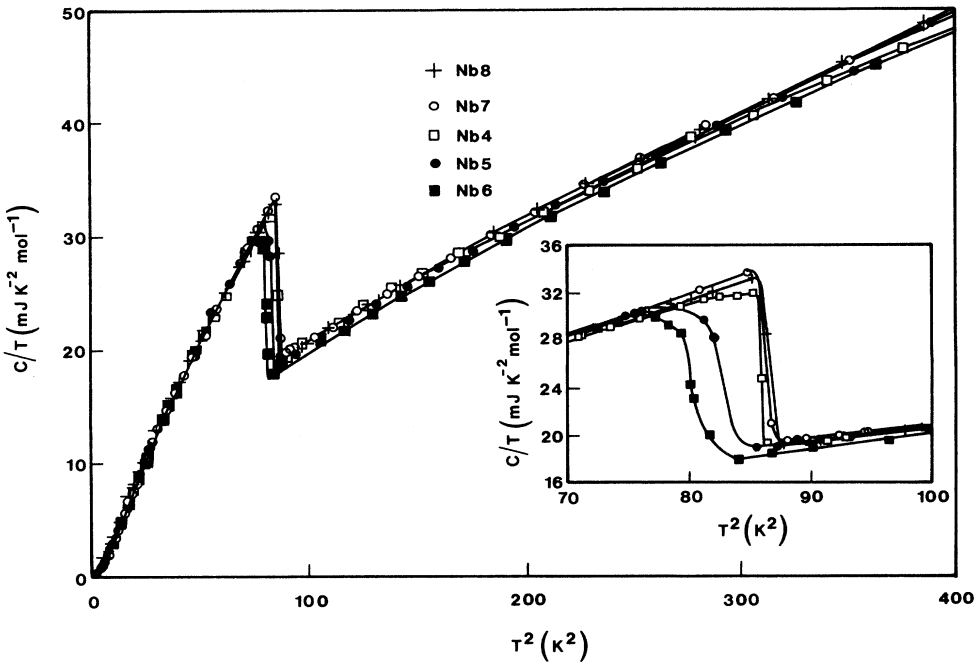

FIG. 6. Specific heat C divided by the temperature T as a function of T^2 for the samples of Table II. Inset: same quantities, expanded scale near the superconducting transition temperature.

tion. Such constraints (to be detailed below) are given by the continuity of the normal-state specific heat and its first derivative at T_c, by the entropy balance, by the initial Debye temperature at $T = 0$, and by the requirement that the curvature should be consistent with a positive phonon density of states. After having so determined the normal-state specific heat, we shall obtain information on the electron density of states, on the phonon spectrum, on the condensation energy and its variation with temperature, and we shall be in a position to follow the changes in the above quantities as a function of the nitrogen content.

Practically, the elaborate analysis outlined above requires the following three steps.

TABLE II. Calorimetric data: results of the fitting procedure. T_c, bulk superconducting critical temperature, in K, r, rms residual of the least squares fit, in % (T_c - 20 K), γ, Sommerfeld constant, in mJ K^{-2} $mole^{-1}$, ΔC (expt.), experimental value of the jump in the specific heat at T_c, in mJ $K^{-1}mole^{-1}$, ΔC (iso.), theoretical value for ΔC (isotropic model), ΔC (aniso.), theoretical value for ΔC (anisotropic model, $\langle a^2 \rangle = 0.0335$), $\Theta(0)$, initial Debye temperature in K[23], $\mu_0 H_c(0)$ (expt.), thermodynamic critical field at T = 0 in mT derived from experiment, $\mu_0 H_c(0)$ (iso.) and $\mu_0 H_c(0)$ (aniso.), theoretical values for an isotropic and an anisotropic model, respectively, ω_n, nth moment of the PDOS in meV as defined in Eq. (18).

Sample	Nb_8	Nb_7	Nb_4	Nb_5	Nb_6
r	0.4	0.7	0.7	0.6	0.4
T_c (calc.)	9.31	9.29	9.26	9.09	8.96
γ	7.80	7.76	7.40	7.45	7.75
ΔC(expt.)	137.2	138.4	133.0	131.4	125.7
ΔC (iso.)		137.4		129.9	
ΔC (aniso.)		128.9		123.9	
$\Theta(0)$	276.6	276.6	276.6	276.6	276.6
$\mu_0 H_c(0)$ (expt.)	202.5[a]	200.2	197.0	193.5	193.0
$\mu_0 H_c(0)$ (iso.)		201.03		194.03	
$\mu_0 H_c(0)$ (aniso.)		197.88		192.04	
$\frac{\mu_0 H_c(0)}{T_c}$	21.76	21.56	21.27	21.29	21.54
ω_2	19.08	19.07	19.10	19.09	19.10
ω_1	18.39	18.38	18.43	18.41	18.43
ω_{-1}	15.92	15.88	15.97	15.92	16.03
ω_{-2}	13.36	13.24	13.36	13.27	13.52

[a] Note that the most likely value of $\mu_0 H_c(0)$ for sample Nb_8 as determined from integration of the magnetization curve is 198.5 mT.

1. The specific-heat anomaly is idealized to show a true discontinuity at T_c, in order to compensate for the smearing resulting both from experimental resolution and possibly from material inhomogeneity. This requires short extrapolations from the regions just below and just above T_c. The idealized step temperature is determined from the requirement that the small entropy added just below T_c in the peak exactly balances the entropy removed just above T_c in the tail. This correction is useful in determining T_c, the specific-heat jump, and the shape of the deviation function close to T_c (cf. Sec. IV C). It does not affect the internal energy at T_c (and therefore the condensation energy) within $4(\delta T/T_c)^2$, where δT is the transition width.

The data of Fig. 6 are shown before this idealization process. The results for T_c defined in this way differ somewhat from the data determined from the magnetization curve (cf. Table II).

2. The data at the low end of the superconducting range are fitted to a polynomial, $C = aT^3 + bT^5$, up to a temperature $T_2 \ll T_c$. The entropy at the lowest measured temperature T_1 is then given by $S_1 = (1/3)aT_1^3 + (1/5)bT_1^5$. The entropy is then obtained by numerical integration of the data from T_1 to T_c. The initial choice of the fitting range (T_2) does not affect the result by more than 0.01% ($1.5 \leq T_2 \leq 1.8$ K).

3. The total specific heat in the normal state is assumed to originate from an electronic term $C_e = \gamma T$ (no variation of γ is allowed which is certainly an approximation in view of the temperature-dependent renormalization) and from a lattice contribution due to the sum of three partial Debye-type phonon spectra $F_i(\omega)$:

$$F_i(\omega) = \begin{cases} 3D_i\omega^2\omega_i^{-3}, & 0 \leq \omega \leq \omega_i, \quad i = 1,2,3 \\ 0 \quad \text{elsewhere.} \end{cases} \tag{16}$$

A nonlinear least-squares program refines all seven parameters γ, ω_i, and D_i under three constraints:[22] (a) the entropy above T_c should match the measured entropy as determined in point 2 above; (b) the composite phonon density of states $F(\omega)$ is normalized, i.e., $D_1 + D_2 + D_3 = 1$; and (c) the initial Debye temperature $\Theta(0)$ given by the composite spectrum, i.e.,

$$D_1\omega_1^{-3} + D_2\omega_2^{-3} + D_3\omega_3^{-3} = \hbar^3 k_B^{-3}\Theta^{-3}(0) \tag{17}$$

is made consistent with the result based on the elastic constants,[23] i.e., $\Theta(0) = 276.6$ K. Of course, the parametrized form of the phonon density allows for a variation of Θ with T.

The final rms difference between the parametrized fit and the normal-state data above T_c amounts to 0.37% (T_c – 20 K) and to 0.57% (T_c – 50 K) in the case of the single crystal. For the sake of consistency in the comparisons, Table II contains the results of the fits up to 20 K only, even for the single crystal. A previous publication[24] using the same data was focused primarily on the properties of "ideal" niobium and the information given by the full fit (T_c – 50 K) was retained. This explains the minor discrepancies (< 1%) with the present data.

Some properties of the phonon density of states (PDOS) obtained by this procedure should be mentioned. Firstly, it reproduces the "kink" in the normal state heat capacity data near 3 K, which has been observed by direct measurements under suitable magnetic fields.[22] Secondly, the main feature of the substitution spectrum $F(\omega)$ is a broad excess PDOS, geometrically centered at ≈ 3 meV and containing about 14% of the modes. This causes a minimum in the effective Debye temperature near 8 K. Thirdly, the fitted spectrum $F(\omega)$ has the correct weight, i.e., the moments of nth order, defined by

$$\omega_n = \langle\omega^n\rangle^{1/n} = \left(\frac{\int d\omega\, \omega^n F(\omega)}{\int d\omega\, F(\omega)}\right)^{1/n} \tag{18}$$

agree with results based on neutron scattering experiments[25] to within 2% ($-2 \leq n \leq 2$).

Once the normal-state specific heat has been determined by the procedure outlined above, various functionals of the specific-heat difference, $C_s - C_n$, between the superconducting and the normal states are readily obtained, e.g., the thermodynamic critical field $H_c(T)$:

$$\frac{\mu_0 V_m H_c^2(T)}{2} = \int_T^{T_c} dT' \, [C_s(T') - C_n(T')]\,[1 - T/T'] \, , \tag{19}$$

where $V_m = 10.825\,\text{cm}^3/\text{mole}$. A selection of data is listed in Table II. Other data for the single crystal are given in Ref. 24.

For the purpose of this paper we emphasize the following results. (1) The sharpness of the specific-heat jump before idealization indicates that interstitial nitrogen is distributed homogeneously within the sample volume. (2) The moments of the PDOS are remarkably constant (±1%) throughout the series. Significant hardening is found only in the most heavily doped sample. The T_c depression is not an effect of phonon shifts. (3) The variation of the Sommerfeld constant γ through the series is small ($\gamma = 7.6 \pm 0.2$ mJ K^{-2} mole^{-1}) and uncorrelated with the variation of T_c. Since γ is obtained by an extrapolation technique rather than by a direct measurement, these variations cannot be considered significant. Furthermore, the thermodynamic critical field $H_c(0)$ decreases monotonously with doping, and closely follows the variation of T_c which is expected in the BCS limit, since $\mu_0 V_m H_c^2/(\gamma T_c^2)$ is a universal constant. The scaling observed between H_c and T_c (within ±1.2%, see Table II) indicates again, that γ is indeed constant throughout the series. H_c is less affected by extrapolation errors than γ for technical reasons. As can be seen from Eq. (19) and from the approximate two-fluid behavior, the major contribution to $H_c(0)$ comes from the upper half of the range of integration where a continuation of the normal-state data is most reliable. We can safely conclude that the T_c depression is not due to a variation of the electronic density of states at the Fermi level.

IV. RESULTS, ANALYSIS, AND DISCUSSION

A. Critical temperatures

As variations in the electronic density of states were ruled out as an explanation for the T_c depression with

increasing nitrogen content, we find another plausible explanation in the smearing out of the anisotropy in the electron-phonon interaction. This possibility has been investigated theoretically by Markowitz and Kadanoff[26] using a separable model to describe the anisotropy of the BCS coupling potential. We have expanded this model to describe an anisotropic electron-phonon interaction spectral function:

$$[\alpha^2 F(\omega)]_{\mathbf{k},\mathbf{k}'} = (1 + a_{\mathbf{k}})\alpha^2 F(\omega)(1 + a_{\mathbf{k}'}), \tag{20}$$

where $\mathbf{k}$ and $\mathbf{k}'$ are the incoming and outgoing quasiparticle momentum vectors in the electron-phonon scattering process and $a_{\mathbf{k}}$ is an anisotropy function which describes the deviation of the anisotropic spectral function, $[\alpha^2 F(\omega)]_{\mathbf{k},\mathbf{k}'}$, from the isotropic one, $\alpha^2 F(\omega)$, in the direction of $\mathbf{k}$. $a_{\mathbf{k}}$ has the important feature

$$\langle a_{\mathbf{k}} \rangle = 0, \tag{21}$$

where $\langle \cdots \rangle$ indicates a Fermi surface average.

The critical temperature is then calculated from a set of anisotropic Eliashberg equations in an imaginary-axis representation[27,28]

$$\tilde{\omega}_{\mathbf{k}}(n) = \omega_n + \pi T_c \sum_{m=-\infty}^{\infty} \left\langle \lambda_{\mathbf{k},\mathbf{k}'}(m-n) + \delta_{m,n} \frac{t^+_{\mathbf{k},\mathbf{k}'}}{T_c} \operatorname{sgn}\tilde{\omega}_{\mathbf{k}'}(m) \right\rangle' ,$$

$$\tilde{\Delta}_{\mathbf{k}}(n) = \pi T_c \sum_{\omega_c} \left\langle \left(\lambda_{\mathbf{k},\mathbf{k}'}(m-n) - \mu^*_{\mathbf{k},\mathbf{k}'} + \delta_{m,n} \frac{t^+_{\mathbf{k},\mathbf{k}'}}{T_c} \right) \frac{\tilde{\Delta}_{\mathbf{k}'}(m)}{|\tilde{\omega}_{\mathbf{k}'}(m)|} \right\rangle' , \tag{22}$$

for the renormalized quasiparticle frequencies $\tilde{\omega}_{\mathbf{k}}(n)$ and the Matsubara gaps $\tilde{\Delta}_{\mathbf{k}}(n)$. $\omega_n = \pi T(2n+1)$ with $n = 0, \pm 1, \pm 2, \ldots$, $\mu^*_{\mathbf{k},\mathbf{k}'}$ is the anisotropic Coulomb interaction pseudopotential, ω_c is the cutoff frequency, $t^+_{\mathbf{k},\mathbf{k}'}$ is defined by

$$t^+_{\mathbf{k},\mathbf{k}'} = \frac{1}{2\pi(\tau_{tr})_{\mathbf{k},\mathbf{k}'}}, \tag{23}$$

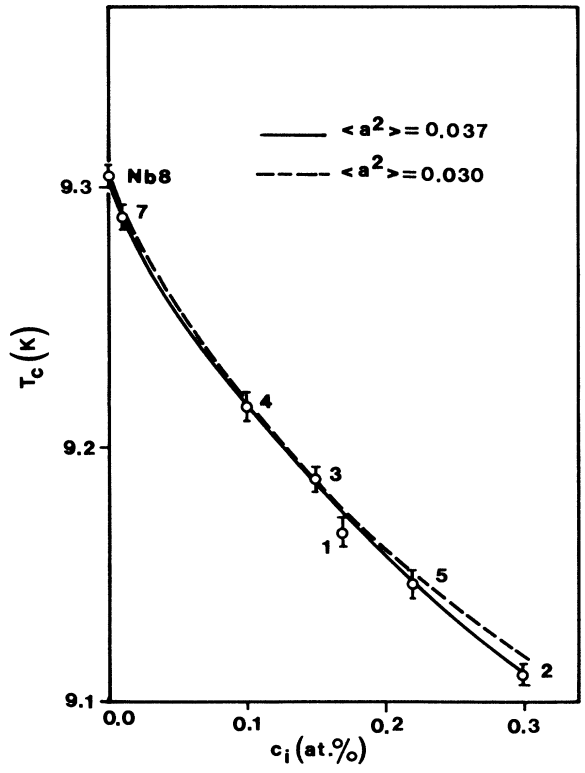

FIG. 7. T_c depression as a function of nitrogen content c_i. The symbols with error bars represent the experimental data while the two full curves represent theoretical results from the solution of Eq. (22) for two values of $\langle a^2 \rangle$.

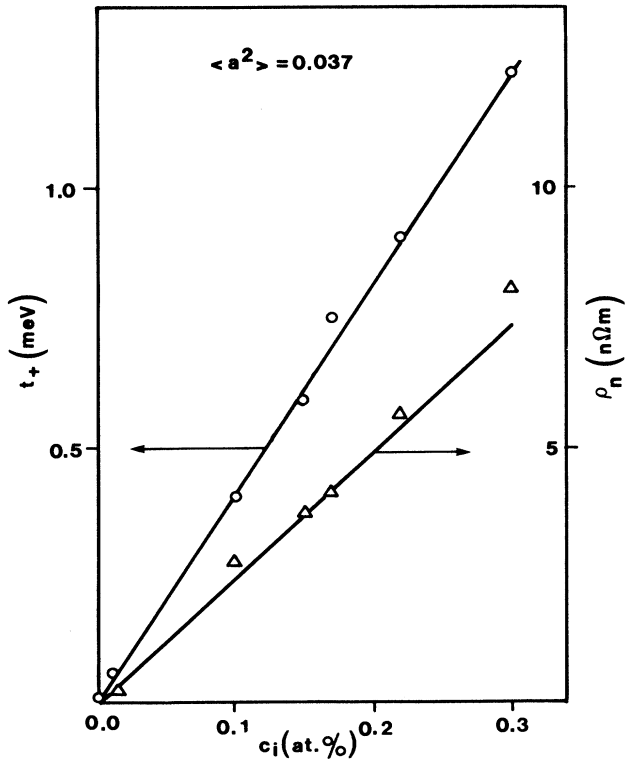

FIG. 8. t^+ and ρ_n as a function of impurity content c_i for $\langle a^2 \rangle = 0.037$. This graph clearly shows the linear relation between the scattering parameter t^+, the residual resistivity ρ_n, and the nitrogen content.

where $(\tau_{tr})_{\mathbf{k},\mathbf{k}'}$ is the anisotropic transport relaxation time, due to impurity scattering, and

$$\lambda_{\mathbf{k},\mathbf{k}'}(m-n) = 2\int_0^\infty \mathrm{d}\omega \frac{[\alpha^2 F(\omega)]_{\mathbf{k},\mathbf{k}'}}{\omega^2 + (\omega_m - \omega_m)^2}. \quad (24)$$

For weak anisotropies, the $\mathbf{k},\mathbf{k}'$ dependence of $\mu^*_{\mathbf{k},\mathbf{k}'}$ and $t^+_{\mathbf{k},\mathbf{k}'}$ can be neglected and the anisotropy of the Matsubara gaps is described by the ansatz

$$\tilde{\Delta}_{\mathbf{k}}(n) = \tilde{\Delta}_0(n) + a_{\mathbf{k}}\tilde{\Delta}_1(n), \quad (25)$$

with $\tilde{\Delta}_{0,1}(n)$ being isotropic.

Equation (25) is applied to Eq. (22) and only terms of the order of $\langle a^2\rangle$, the mean-square electron-phonon interaction anisotropy, are kept. Furthermore, the isotropic Coulomb pseudopotential and the isotropic transport relaxation time are described by the parameters μ^* and $t^+ = 1/(2\pi\tau_{tr})$, respectively.

The experimental data describing the depression of T_c with increasing nitrogen content are then used to fit the value of $\langle a^2\rangle$. For this procedure we assume the clean limit ($t^+ = 0$) critical temperature of niobium to be 9.305 K, slightly higher than the critical temperature of the high purity single crystal sample Nb_8. Furthermore, we use the $\alpha^2F(\omega)$ spectrum measured by Arnold *et al.*[29] which has a mass enhancement factor $\lambda = 1$, and we choose the cutoff to be $6\omega_D = 174$ meV.

Figure 7 shows the result of such a fitting procedure and it becomes obvious that $\langle a^2\rangle = 0.03$ and 0.037 fit the data equally well. Thus, we can assume that these two numbers establish a lower and an upper limit for the mean-square anisotropy of the electron-phonon coupling. Of course, for each value of $\langle a^2\rangle$ we find a different value of μ^* to give the clean limit T_c ($\mu^* = 0.204$ for $\langle a^2\rangle = 0.037$) and each impurity concentration results in a particular value of t^+. Figure 8 shows this for $\langle a^2\rangle = 0.037$ and it is essential that $t^+ \sim n_I$, the nitrogen concentration. The same holds for the residual resistivity.

B. Upper critical fields, H_{c2}

It has already been observed by Sauerzopf *et al.*[7] that the high purity single crystal sample Nb_8 exhibits a pronounced anisotropy of the upper critical field H_{c2} as a function of the orientation of the crystal axis with respect to the applied external magnetic field. Furthermore, Hohenberg and Werthamer[30] pointed out that anisotropy effects in polycrystalline samples manifest themselves in an upward curvature of $H_{c2}(T)$ near T_c, which is clearly observed by experiment (cf. Fig. 9 below).

The theory of $H_{c2}(T)$ for anisotropic polycrystalline superconductors in a separable model scheme was developed by Prohammer and Schachinger.[31] It employs the separable ansatz (20) for the anisotropy of the electron-phonon interaction and the ansatz

$$v_{F,\mathbf{k}} = (1 + b_{\mathbf{k}})\langle v_F\rangle, \quad (26)$$

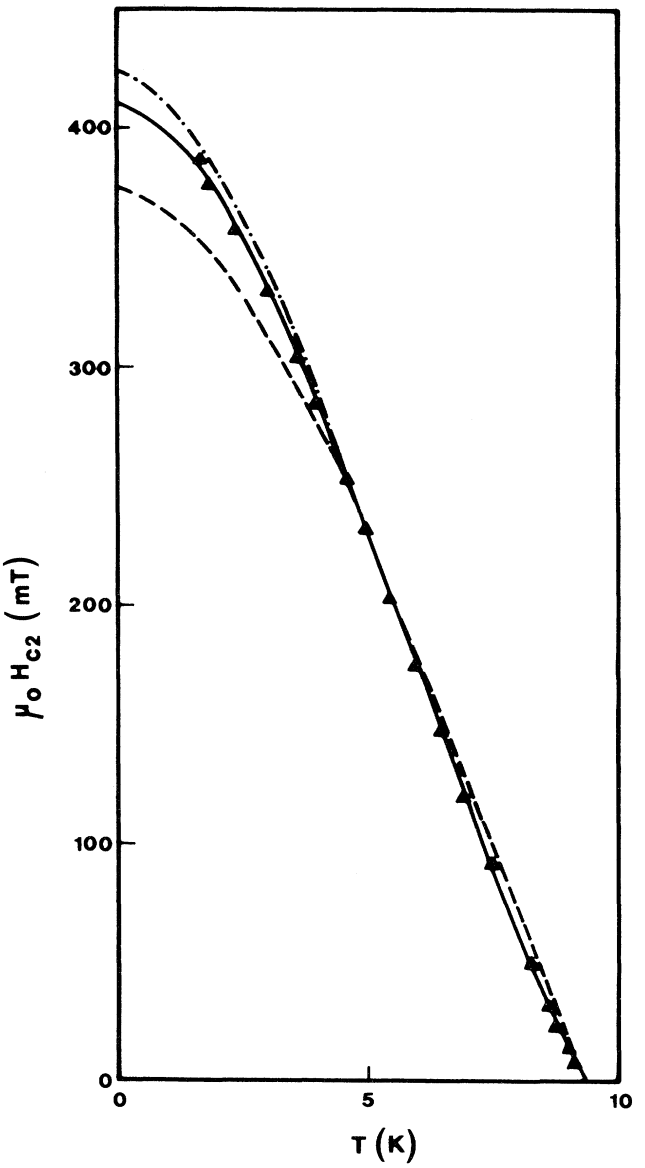

FIG. 9. Results of a fitting procedure for theoretical results calculated from Eqs. (27)–(30) to the experimental data of sample Nb_7. Full line: $\langle a^2\rangle = 0.037$, $\langle b^2\rangle = 0.111$, dashed-dotted line: $\langle a^2\rangle = 0.03$, $\langle b^2\rangle = 0.13$. v_F is in both cases 0.57×10^6 m/s. The dashed line represents the results for an isotropic system with $v_F = 0.42 \times 10^6$ m/s.

which describes the anisotropy of the Fermi velocity.[5] $b_{\mathbf{k}}$ is again an anisotropy function defined in the same way as $a_{\mathbf{k}}$.

The upper critical field is then determined by the following set of equations:

$$\tilde{\omega}_{\mathbf{k}}(n) = \omega_n + \pi T \sum_{m=-\infty}^{\infty} (1 + a_{\mathbf{k}})\,\lambda(m-n)\,\mathrm{sgn}\tilde{\omega}_{\mathbf{k}}(m) + \pi t^+ \mathrm{sgn}\tilde{\omega}_{\mathbf{k}}(n)\,, \quad (27)$$

$$\tilde{\Delta}_{\mathbf{k}}(n) = \pi T \sum_{\omega_c} (1 + a_{\mathbf{k}})\, \lambda(m-n) \left\langle (1 + a_{\mathbf{k}'})\, \tilde{\Delta}_{\mathbf{k}'}(m) \chi_{\mathbf{k}'}(m) \right\rangle' - \pi T \sum_{\omega_c} \left(\mu^* - \delta_{m,n} \frac{t^+}{T} \right) \left\langle \tilde{\Delta}_{\mathbf{k}'}(m) \chi_{\mathbf{k}'}(m) \right\rangle' , \tag{28}$$

$$\chi_{\mathbf{k}}(n) = \frac{2}{\sqrt{\alpha_{\mathbf{k}}}} \int_0^\infty \mathrm{d}q\, e^{-q^2} \tan^{-1} \left(\frac{q\sqrt{\alpha_{\mathbf{k}}}}{|\tilde{\omega}_{\mathbf{k}}(n)|} \right) , \tag{29}$$

and

$$\alpha_{\mathbf{k}} = \frac{e\mu_0}{2} H_{c2}(T) \langle v_F \rangle^2 (1 + b_{\mathbf{k}})^2 . \tag{30}$$

Clearly, this introduces two new parameters, the Fermi surface average of the Fermi velocity $\langle v_F \rangle$ and its mean-square anisotropy $\langle b^2 \rangle$.

These two parameters can be found by fitting the theory to the $H_{c2}(T)$ data measured for one sample, for instance, sample Nb_7, using the values of μ^*, t^+, and $\langle a^2 \rangle$ found earlier, as an input for the calculations. Nevertheless, there is still some ambiguity left in defining $b_{\mathbf{k}}$, which could be in phase with $a_{\mathbf{k}}$ or not. This problem is resolved by the experimental de Haas–van Alphen results reported by Crabtree *et al.*[32] who convincingly showed (in their Fig. 14) that $b_{\mathbf{k}}$ and $a_{\mathbf{k}}$ have opposite signs on the Fermi surface, making v_F small where the electron-phonon coupling is strong and vice versa.

The fitting procedure is very sensitive to the choice of the anisotropy parameters, as is demonstrated in Fig. 9. The values for $\langle v_F \rangle$ and $\langle b^2 \rangle$ for a given set of data for $\langle a^2 \rangle$, μ^*, and t^+ are chosen to reproduce in an optimal way the high temperature tail of the $H_{c2}(T)$ curve. It becomes quite obvious that the low-temperature part of the $H_{c2}(T)$ curve can then be used to find the best set of parameters in order to reproduce the temperature dependence of the upper critical field over the whole temperature range. This results in one set of data, $\langle a^2 \rangle$, $\langle b^2 \rangle$, $\langle v_F \rangle$, and μ^* describing the intrinsic normal state properties of niobium, which should not change by changing the impurity content of the sample. Thus, using the appropriate value for t^+, the theory has no further adjustable parameter and should, in principle, reproduce the experimental $H_{c2}(T)$ data of all the other samples.

Nevertheless, we have already experienced some ambiguity in determining $\langle a^2 \rangle$ which resulted in an upper and a lower limit of this parameter. Therefore, it is only natural to apply the above procedure to each individual sample in order to establish upper and lower limits of $\langle b^2 \rangle$ and $\langle v_F \rangle$. Maximum accuracy is achieved if this is done using the anisotropy deviation function

$$D_a(t) = 100 \left(\frac{H_{c2}^a(t)}{H_{c2}^i(t)} - 1 \right) ; \qquad t = T/T_c . \tag{31}$$

$H_{c2}^a(t)$ is the upper critical field of the anisotropic polycrystal and $H_{c2}^i(t)$ is the upper critical field of a *theoretical* isotropic system having the same T_c, t^+, $\langle v_F \rangle$, and $\alpha^2 F(\omega)$ as the real anisotropic system. Figure 10 shows the results of such a procedure for the deviation function and Table I quotes the results which suggest the following limits:

$$\begin{aligned} \langle a^2 \rangle &= 0.0335 \pm 0.0035 , \\ \langle b^2 \rangle &= 0.118 \pm 0.007 , \\ \langle v_F \rangle &= 0.57 \pm 0.01 \times 10^6 \text{ m/s}. \end{aligned} \tag{32}$$

If we recalculate $D_a(t)$ using the average values quoted above we get the results presented in Fig. 11. The maximum deviation between theory and experiment of about

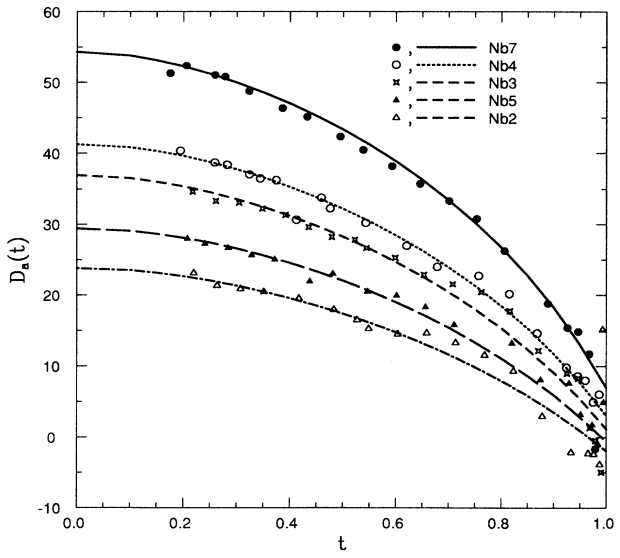

FIG. 10. The anisotropy deviation function $D_a(t)$ for the best possible fit for each individual sample. The corresponding values for the anisotropy parameters and v_F are listed in Table I.

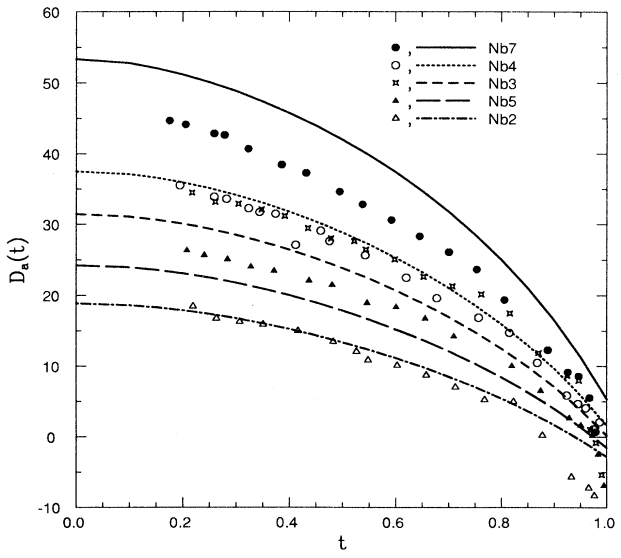

FIG. 11. The anisotropy deviation function D_a for the anisotropy parameters and v_F according to Eq. (32).

12 percentage points is found for sample Nb_7 at low temperatures. All the other polycrystalline samples show deviations smaller than 5 percentage points. This corresponds to a maximum error of less than 2 % in the reproduction of the experimental $H_{c2}(T)$ data for all samples over the whole temperature range, if the parameters of Eq. (32) are used.

Figure 12 finally shows how the upward curvature of $H_{c2}(T)$ at T_c is reproduced by theory and how this curvature becomes less pronounced with increasing nitrogen concentration as a result of smearing out the anisotropy.

C. Thermodynamics

The thermodynamics of a superconductor is calculated from the free energy difference ΔF between the normal and the superconducting states:[33]

$$\Delta F = N(0)\pi T \sum_{\omega_c} \left\langle \left(\sqrt{\tilde{\Delta}_{\mathbf{k}}^2(n) + \tilde{\omega}_{\mathbf{k}}^2(n)} - |\tilde{\omega}_{\mathbf{k}}(n)| \right) \left(1 - \frac{|\tilde{\omega}_{\mathbf{k}}^0(n)|}{\sqrt{\tilde{\Delta}_{\mathbf{k}}^2(n) + \tilde{\omega}_{\mathbf{k}}^2(n)}} \right) \right\rangle, \tag{33}$$

where the $\tilde{\omega}_{\mathbf{k}}(n)$ and $\tilde{\Delta}_{\mathbf{k}}(n)$ are the solutions of the nonlinear anisotropic Eliashberg equations:

$$\begin{aligned} \tilde{\omega}_{\mathbf{k}}(n) &= \omega_n + \pi T \sum_{m=-\infty}^{\infty} \left\langle \lambda_{\mathbf{k},\mathbf{k}'}(m-n) + \delta_{m,n} \frac{t_{\mathbf{k},\mathbf{k}'}^+}{T} \frac{\tilde{\omega}_{\mathbf{k}'}(m)}{\sqrt{\tilde{\Delta}_{\mathbf{k}'}^2(m) + \tilde{\omega}_{\mathbf{k}'}^2(m)}} \right\rangle', \\ \tilde{\Delta}_{\mathbf{k}}(n) &= \pi T \sum_{\omega_c} \left\langle \left(\lambda_{\mathbf{k},\mathbf{k}'}(m-n) - \mu_{\mathbf{k},\mathbf{k}'}^* + \delta_{m,n} \frac{t_{\mathbf{k},\mathbf{k}'}^+}{T} \right) \frac{\tilde{\Delta}_{\mathbf{k}'}(m)}{\sqrt{\tilde{\Delta}_{\mathbf{k}'}^2(m) + \tilde{\omega}_{\mathbf{k}'}^2(m)}} \right\rangle', \end{aligned} \tag{34}$$

and $\tilde{\omega}_{\mathbf{k}}^0(n)$ is determined from

$$\tilde{\omega}_{\mathbf{k}}^0(n) = \omega_n + \pi T \sum_{m=-\infty}^{\infty} \left\langle \lambda_{\mathbf{k},\mathbf{k}'}(m-n) + \delta_{m,n} \frac{t_{\mathbf{k},\mathbf{k}'}^+}{T} \right\rangle' \operatorname{sgn}\omega_m. \tag{35}$$

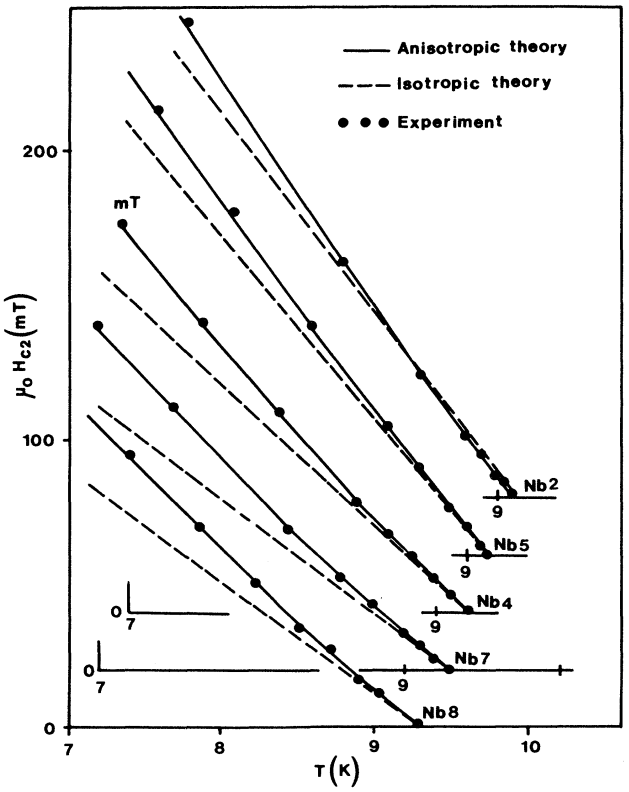

FIG. 12. High temperature tails of the $H_{c2}(T)$ curves and their reproduction by theory (solid line). The dashed lines reproduce the best possible fit for an isotropic model calculation.

The thermodynamic critical field is then given by

$$H_c(T) = \sqrt{2\Delta F(T)/\mu_0} \tag{36}$$

and the specific-heat difference by

$$\Delta C(T) = -T \frac{\partial^2 \Delta F(T)}{\partial T^2}. \tag{37}$$

It is obvious from Eq. (33) that only $\langle a^2 \rangle$ matters and as this parameter is already determined, there are no adjustable parameters left.

From a theoretical point of view, it is certainly preferable to compare theoretical thermodynamic critical field data with experiment. This proved to be very successful in the case of the type-I superconductor indium,[34] where the influence of the anisotropy in the electron- phonon interaction was clearly observable. As niobium is a type-II superconductor, $H_c(T)$ is not directly accessible to experiment and has to be calculated either from an integration of the magnetization curve or from an integration of the specific heat data [Eq. (19)].

Nevertheless, we would like to present results for the magnetic deviation function

$$D_H(t) = \frac{H_c(t)}{H_c(0)} - (1 - t^2) \tag{38}$$

for at least one sample, the high purity single crystal sample Nb_8. The extrapolation of the experimental $H_c(T)$ data to $T = 0$ results in a $H_c(0)$ between 197.0 and 200.5 mT. Figure 13 compares the experimental data [open circles, $\mu_0 H_c(0) = 198.5$ mT] with theoretical predictions. Even with the large error bar attached to the experimen-

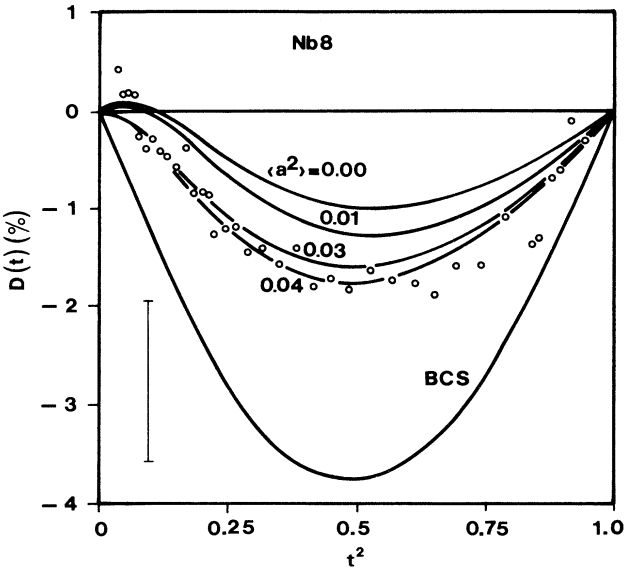

FIG. 13. Magnetic deviation function $D_H(t)$ according to Eq. (38) for the pure single crystal sample Nb_8. The open circles represent experimental data calculated for $\mu_0 H_c(0) = 198.5$ mT. The solid curves represent theoretical predictions from BCS theory and anisotropic Eliashberg theory (labeled by different values of $\langle a^2 \rangle$).

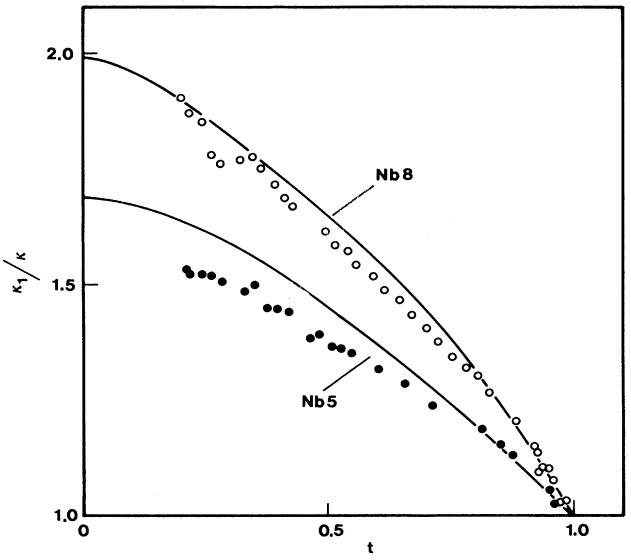

FIG. 14. Temperature dependence of the generalized Ginzburg - Landau parameter κ_1 in pure (Nb_8) and dirty (Nb_5) niobium. The solid lines represent the results of anisotropic Eliashberg theory with $\langle a^2 \rangle = 0.037$, $\langle b^2 \rangle = 0.112$, and $v_F = 0.585 \times 10^6$ m/s for sample Nb_8, and $\langle a^2 \rangle = 0.034$, $\langle b^2 \rangle = 0.125$, and $v_F = 0.558 \times 10^6$ m/s for sample Nb_5.

tal data, it becomes obvious that the BCS result is far off. The other full curves labeled with different values for $\langle a^2 \rangle$ result from anisotropic Eliashberg theory and show a reasonably good agreement with experiment. A mean-square anisotropy of the electron-phonon interaction of $0.03 \leq \langle a^2 \rangle \leq 0.04$ seems to be most likely.

This result is furthermore supported by a comparison between experimental $\kappa_1(T)$ [see Eq. (3)] and theoretical predictions generated using the results of Table I. Figure 14 presents results for the two samples Nb_8 and Nb_5. The agreement is excellent for the clean sample (Nb_8), with the experimental data falling slightly below the theoretical predictions. This becomes more pronounced in the case of the dirty sample (Nb_5). For this sample, small residual hysteresis effects were found to become increasingly more significant at low temperatures. Therefore, the observed discrepancy between theory and experiment can be related to the evaluation of the thermodynamic critical field $H_c(T)$ from magnetization curves. Increasing irreversibility near the lower critical field H_{c1} shifts the magnetization to higher fields and this in turn results in higher H_c values and consequently in smaller $\kappa_1(T)$ values.

On the other hand, the specific-heat difference can be calculated from two successive differentiations of the theoretical free energy data, a procedure which makes the convergence requirements for the solution of the Eliashberg equations (34) very stringent. It has, therefore, certainly some advantage to use the deviation function of the entropy

$$D_S(T) = \frac{\Delta S(t)}{\gamma T_c} - t(t^2 - 1), \tag{39}$$

where $\Delta S(t)$ is the entropy difference between the superconducting and the normal state and $t(t^2 - 1)$ is just the two-fluid model prediction for the normalized entropy difference. The calculation of $\Delta S(t)$ requires only a single differentiation of the theoretical free-energy difference and a single integration of the experimental specific-heat data where uncertainties can be greatly suppressed by the use of the third principle.

Figures 15(a) and 15(b) compare the experimental data for the samples Nb_7 and Nb_5 with theoretical predictions for the entropy deviation function. In both cases the experimental data (full circles) are closer to the predictions for an isotropic system which is rather surprising. A possible explanation might be found in the fact that the temperature dependence of the mass enhancement factor λ (Ref. 35) is neglected in the analysis of the specific-heat data, because this would result in a temperature dependent γ. In the temperature range $0 \leq T \leq T_c$, λ varies by about 8% which is probably enough to explain the observed discrepancies. Further thermodynamic data are compared for the two samples in Table II. It is interesting to note that for both samples the calorimetrically determined value of $\mu_0 H_c(0)$ is just between the theoretical predictions for the isotropic and the anisotropic systems. The error is in both cases $\sim 1\%$ which gives quite some confidence in the theoretical evaluation of the free energy. Furthermore, it should be pointed out that the most likely values of $H_c(0)$ as determined from magnetization measurements are consistently smaller than the calorimetric ones and very close to the results of the anisotropic theory (cf. above, Fig. 13 and the note in Table II).

All this leads to the conclusion that magnetic mea-

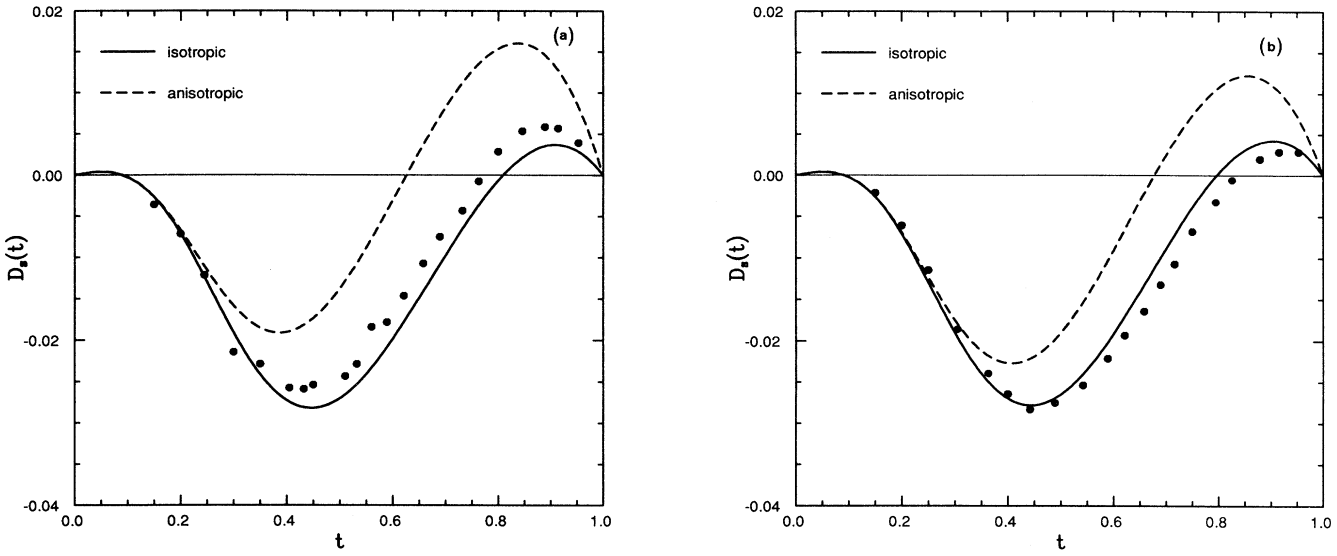

FIG. 15. The entropy deviation function $D_S(t)$ for the samples Nb_7 (a) and Nb_5 (b). The full circles represent the experimental data, the full curve the results for the isotropic model, and the dashed line corresponds to the results of an anisotropic model with $\langle a^2 \rangle = 0.0335$.

surements are more sensitive to anisotropic features of a superconductor than the specific heat measurements.

D. Summary of analysis

We are now in a position to perform various consistency checks. One obvious check would be to compare the results of Eqs. (32) to the de Haas – van Alphen measurements.[32] Figures 16(a) and 16(b) compare our results for the variation of λ and of v_F with the experimental data. In both cases the agreement is exceptionally good and confirms the results of our analysis. Our value for $\langle v_F \rangle$ of 0.57×10^6 m/s is also in very good agreement with the result of Eq. (13) which gives a $\langle v_F \rangle$ of 0.556×10^6 m/s for $\lambda = 1$; band-structure calculations[36] predict $\langle v_F \rangle = 0.62 \times 10^6$ m/s which is in excellent agreement with our value. (In contrast, an analysis of the upper critical field data using an isotropic theory[37] would result only in a $\langle v_F \rangle$ of 0.47×10^6 m/s.)

A further consistency check concerns the comparison of the residual resistivity data ρ_n to theoretical predictions which follow from a Drude theory. We find for the

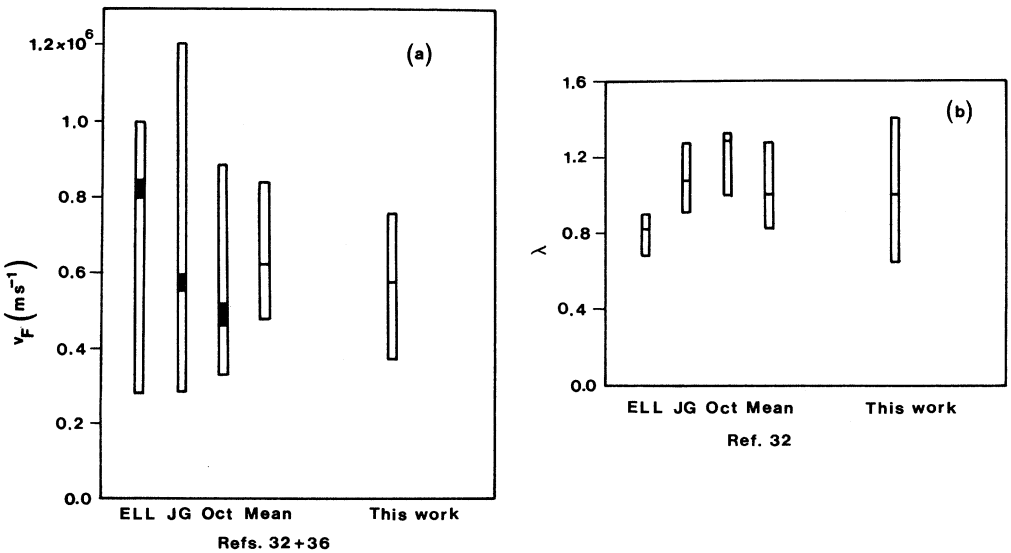

FIG. 16. Comparison of the de Haas – van Alphen results on the anisotropy of (a) v_F and of (b) λ with the results of the theoretical analysis according to Eq. (32). ("Ell" refers to the elliptic, "JG" to the jungle gym, and "Oct" to the octahedron part of the Fermi surface.) The black bar represents the uncertainty in the calculation of the mean value for the various parts of the Fermi surface.

plasma frequency Ω_p the value 8.83 eV and this allows to calculate ρ_{theor} from the transport relaxation time and thus from t^+ according to Eqs. (1) and (23). Table I compares theoretical (ρ_{theor}) and experimental (ρ_n) values and we find again a very good agreement between the theoretical predictions and the experimental data for all samples investigated.

In summary, the theoretical analysis of experimental data for T_c and the upper critical field required a rather moderate anisotropy of the electron-phonon coupling interaction and a quite pronounced anisotropy of the Fermi velocity. This is in contrast to an earlier analysis by Butler[2] who assumed that the anisotropy of the Fermi velocity alone could account for the observed anisotropy effects in niobium.

V. CONCLUSION

We have presented results of a systematic study on the impurity dependence of superconductive and normal state properties in niobium, in order to clarify the role of anisotropies in the electron-phonon coupling strength and the Fermi velocity. The experimental investigations were supplemented by an extensive analysis in terms of anisotropic Eliashberg theory.

With regard to the thermodynamic properties, the impurity dependence of the transition temperature T_c can be assessed accurately from experiment and discussed appropriately in terms of theory on the basis of a separable model for the coupling anisotropy. This has led to a mean-square anisotropy parameter $\langle a^2 \rangle = 0.0335 \pm 0.0035$ for clean niobium. On the other hand, both the thermodynamic critical field deviation function and the specific heat suffer from the small contribution of anisotropy to the experimentally determined temperature and impurity dependence and are, hence, much less suited for a quantitative discussion in terms of theory and, consequently, an unambiguous assessement of anisotropy effects.

On the other hand, the temperature and impurity dependence of H_{c2} have been shown to be ideally suited for this purpose. Based on the recent formulation[31] of an anisotropic Eliashberg theory of the upper critical field H_{c2} and using the coupling anisotropy $\langle a^2 \rangle$ as determined from the T_c depression with impurity content, a mean-square anisotropy of the Fermi velocity ($\langle b^2 \rangle = 0.118 \pm 0.007$) as well as the actual magnitude of $\langle v_F \rangle$ ($= 0.57 \pm 0.01 \times 10^6$ m/s) have been deduced. With these parameters, the temperature dependence of H_{c2} could be described in a most satisfactory way over a wide range of impurity concentrations. The results reflect the "smearing out" of anisotropies with increasing impurity content, a picture, which has been confirmed by the specific-heat measurements independently.

It is the main result of this study that both the anisotropy of the electron-phonon interaction and of the Fermi velocity, can indeed explain the superconducting properties of pure niobium and of impure niobium with dilute impurity concentrations. We conclude, that the anisotropy of the electron-phonon interaction is rather weak and comparable to that of indium.[34] The anisotropy of the Fermi velocity is very pronounced and is comparable to that of Nb_3Sn single crystals.[38] The theoretical analysis proved to be consistent with other normal state properties of niobium like the residual resistivity or the anisotropy of the Fermi velocity as observed by de Haas–van Alphen experiments.[32]

ACKNOWLEDGMENTS

We wish to thank Dr. F.M. Sauerzopf and Dr. M. Botlo for many helpful discussions and H. Niedermaier for his help with the experiments. This work was supported in part by Fonds zur Förderung der Wissenschaftlichen Forschung, Wien, under Contract Nos. 3973, 5032, 6067, and 6078P.

[1] M. Peter, J. Ashkenazi, and M. Dacorogna, Helv. Phys. Acta **50**, 267 (1977).
[2] W.H. Butler, Phys. Rev. Lett. **44**, 1516 (1980).
[3] G. Eilenberger and V. Ambegaokar, Phys. Rev. **158**, 332 (1967).
[4] H.R. Kerchner, D.K. Christen, and S.T. Sekula, Phys. Rev. B **21**, 86 (1980).
[5] H. Teichler, in *Anisotropy Effects in Superconductors*, edited by H.W. Weber (Plenum, New York, 1977), p. 75, and references therein.
[6] E. Seidl, H.W. Weber, and H. Teichler, J. Low Temp. Phys. **37**, 639 (1979).
[7] F.M. Sauerzopf, E. Moser, H.W. Weber, and F.A. Schmidt, J. Low Temp. Phys. **66**, 191 (1987).
[8] S.T. Sekula and R.H. Kernohan, Phys. Rev. B **9**, 904 (1972).
[9] B. Vlcek, E. Seidl, H.W. Weber, E. Schachinger, and W. Pint, Physica C **167**, 198 (1990).
[10] P. Hahn and H.W. Weber, Cryogenics **23**, 87 (1983).
[11] H.W. Weber, E. Seidl, M. Botlo, C. Laa, E. Mayerhofer, F.M. Sauerzopf, R.M. Schalk, A.P. Wiesinger, and J. Rammer, Physica C **161**, 272 (1989).
[12] H.W. Weber, E. Seidl, M. Botlo, C. Laa, H.P. Wiesinger, and J. Rammer, Physica C **161**, 287 (1989).
[13] E. Seidl, C. Laa, H.P. Wiesinger, H.W. Weber, J. Rammer, and E. Schachinger, Physica C **161**, 294 (1989).
[14] M. Botlo, H.W. Weber, and U. Klein, in *Proceedings of the 17th International Conference on Low Temperature Physics*, edited by U. Eckern, A. Schmid, W. Weber, and H. Wühl (North-Holland, Amsterdam, 1984), p. 1285.
[15] R.A. French, Cryogenics **8**, 301 (1968).
[16] E. Seidl, C. Laa, H.P. Wiesinger, H.W. Weber, J. Rammer, and E. Schachinger, Physica C **161**, 294 (1989).
[17] B.B. Goodman, IBM J. Res. Dev. **6**, 63 (1962).
[18] C.P. Gor'kov, Zh. Eksp. Teor. Fiz. **36**, 1918 (1959) [Sov. Phys. JETP **9**, 1366 (1959)].
[19] D.K. Finnemore, T.F. Stromberg, and C.A. Swenson, Phys. Rev. **149**, 231 (1966).
[20] C.G.B. Baker, E.M. Forgan, and C.E. Gough, Physica B **108**, 927 (1981).

[21] M.A. Moore and D.I. Paul, Solid State Commun. **9**, 1303 (1971).
[22] A. Junod, D. Bichsel, and J. Muller, Helv. Phys. Acta **52**, 580 (1979).
[23] R. Wanner, Can. J. Phys. **48**, 1270 (1970).
[24] A. Junod, J.-L. Jorda, and J. Muller, J. Low Temp. Phys. **62**, 301 (1986).
[25] Y. Nakagawa and A.D.B. Woods, Phys. Rev. Lett. **11**, 271 (1963).
[26] D. Markowitz and L.P. Kadanoff, Phys. Rev. **131**, 563 (1963).
[27] J.P. Carbotte, Rev. Mod. Phys. **62**, 1027 (1990).
[28] J.M. Daams and J.P. Carbotte, J. Low Temp. Phys. **43**, 263 (1981).
[29] G.B. Arnold, J. Zasadzinski, J.W. Osmun, and E.L. Wolf, J. Low Temp. Phys. **40**, 225 (1980).
[30] P.C. Hohenberg and N.R. Werthamer, Phys. Rev. **153**, 493 (1967).
[31] M. Prohammer and E. Schachinger, Phys. Rev. B **36**, 8353 (1987).
[32] G.W. Crabtree, D.H. Dye, D.P. Karim, S.A. Campbell, and J.B. Ketterson, Phys. Rev. B **35**, 1728 (1987).
[33] J. Bardeen and M. Stephen, Phys. Rev. **136**, A1485 (1964).
[34] L. Niel, N. Giesinger, H.W. Weber, and E. Schachinger, Phys. Rev. B **32**, 2976 (1985).
[35] G. Grimvall, J. Phys. Chem. Solids **29**, 1221 (1968).
[36] L.F. Mattheiss, Phys. Rev. B **1**, 373 (1970).
[37] M. Schossmann and E. Schachinger, Phys. Rev. B **33**, 6123 (1986).
[38] E. Schachinger and M. Prohammer, Physica C **156**, 701 (1988).